

Self-Supervised Learning based on Transformed Image Reconstruction for Equivariance-Coherent Feature Representation

Qin Wang¹ Benjamin Bruns¹ Hanno Scharr¹ Kai Krajsek²

¹IAS-8: Data Analytics and Machine Learning, Forschungszentrum Jülich, Germany

²Jülich Supercomputing Centre (JSC), Forschungszentrum Jülich, Germany
 {qi.wang, b.brunns, k.krajsek, h.scharr}@fz-juelich.de

Abstract

The equivariant behaviour of features is essential in many computer vision tasks, yet popular self-supervised learning (SSL) methods tend to constrain equivariance by design. We propose a self-supervised learning approach where the system learns transformations independently by reconstructing images that have undergone previously unseen transformations. Specifically, the model is tasked to reconstruct intermediate transformed images, e.g. translated or rotated images, without prior knowledge of these transformations. This auxiliary task encourages the model to develop equivariance-coherent features without relying on predefined transformation rules. To this end, we apply transformations to the input image, generating an image pair, and then split the extracted features into two sets per image. One set is used with a usual SSL loss encouraging invariance, the other with our loss based on the auxiliary task to reconstruct the intermediate transformed images. Our loss and the SSL loss are linearly combined with weighted terms. Evaluating on synthetic tasks with natural images, our proposed method strongly outperforms all competitors, regardless of whether they are designed to learn equivariance. Furthermore, when trained alongside augmentation-based methods as the invariance tasks, such as iBOT or DINOv2, we successfully learn a balanced combination of invariant and equivariant features. Our approach performs strong on a rich set of realistic computer vision downstream tasks, almost always improving over all baselines.

1. Introduction

We introduce a self-supervised learning (SSL) auxiliary task based on reconstruction of transformed images that improves learning of equivariance-coherent feature representations. For a schematic overview see Figure 1.

Leveraging unannotated images for image representation learning through SSL [2, 8, 9, 22, 24, 33, 45] methods is

crucial for pretraining foundation models. However, most SSL methods, including e.g. the popular DINOv2 [33], are based on surrogate tasks, supporting invariance of learned features with respect to augmentations of the inputs. In addition, the most common evaluation metric for SSL in computer vision is image classification by linear probing on ImageNet-1K [12], a task with labels being invariant under image transformations used for augmentation. Consequently, SSL methods are primarily evaluated for suitability of their invariant features. For downstream tasks relying on equivariance, this may not be the best approach.

Equivariance in feature learning ensures that a model’s learned representations remain consistent under various transformations, including 2D or 3D translations, rotations, scaling, and changes in colour or illumination. ‘Equivariance’ means that the information about the transformation can still be retrieved from the feature representation. In convolutional neural networks (CNNs) [35], translation equivariance is achieved using convolutional layers. This property is useful in tasks like object detection and image segmentation where transformation awareness (e.g., estimating the position and orientation of an object) is critical.

As we show, current SSL methods exhibit suboptimal performance on tasks related to equivariance, such as the synthetic task in Figure 2, primarily due to their reliance on augmentation-invariant approaches. We heal this deficit by applying our auxiliary task to a fraction z_{equi} of the features and show that this allows to improve performance consistently, not only for synthetic equivariant downstream tasks, but also even for tasks associated with feature invariance.

Our contribution

- We introduce an augmentation-based SSL loss enhancing equivariant behavior of learned features.
- Our approach strongly outperforms competitors on all synthetic equivariance test tasks from [36].
- Our approach performs strong on a wide range of computer vision tasks compared to iBOT [45] and DINOv2 [33], improving performance in almost all cases and

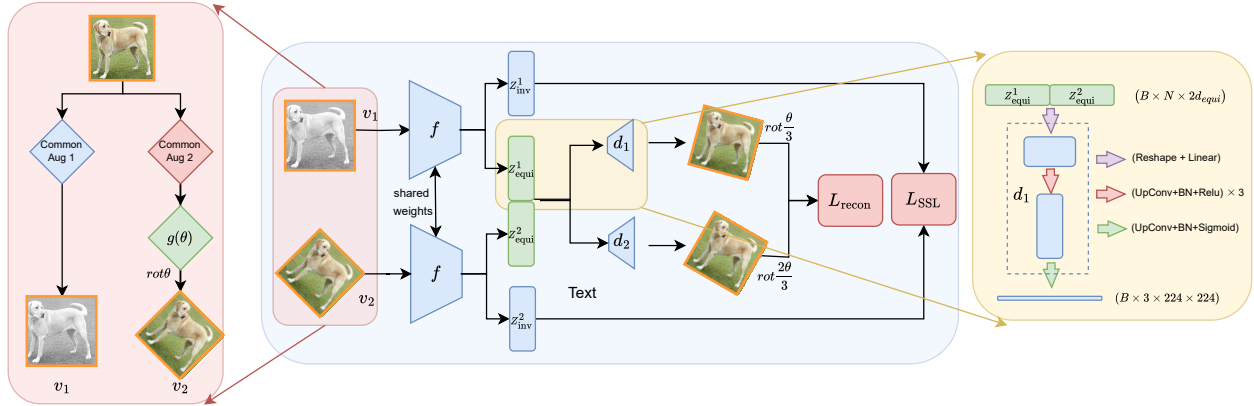


Figure 1. **Overview of our proposed framework.** Transformation g with example of rotation with angle θ . The common augmentation pipeline is as DINOv2, but on v_2 , a transformation is applied along with common augmentation.

clearly improving on average, where other equivariance-enhancing approaches underperform.

2. Related work

2.1. Equivariant neural networks

Since the early days of neural networks research, the exploration of symmetries in the data has played a significant role, reduced model complexity, and improved inference quality of models [16]. One might argue that without convolutional neural networks, inherently implementing approximately translational equivariance, computer vision models could not have made this progress in the field. However, built-in permutation equivariance in transformer architectures has also been the object of study [41]. Not surprisingly, equivariance in deep learning is a vivid research field which we define into sub-categories: those that study models that inherit built-in equivariance [10, 26] and models that gain this property by experience [11, 37, 39].

2.2. Self-supervised learning

State-of-the-art self-supervised learning (SSL) methods learn feature representations by automatically labelling non-labeled data and applying supervised learning techniques. The assumption is that the learned feature representation is comprehensive enough to be used later in other tasks, denoted as downstream tasks. A large variety of different SSL methods have been proposed [5, 7–9, 22, 23, 29, 33, 40, 42] and they can be classified with different metrics. For an overview, we refer to [3]. The relevant metric for our purpose is how models react to different transformations in the input space, *i.e.*, if they maintain the information in the feature representation or if this information is lost or partly lost. Older SSL methods proposed auxiliary tasks such as Jigsaw puzzle [32] or rotation

estimation [19] that foster equivariance properties as the transformation properties need to be maintained in feature space. These methods have been overtaken by matching-type methods that present two different versions of the same semantic content to the model and motivate it to map these two versions to nearby points in feature space. Semantically different images are mapped to points far apart. This is achieved either by contrastive learning approaches or by regularisation techniques like de-correlation [5, 42] or teacher-student architectures [33, 45]. Consequently, these matching-type methods learn feature representations that suppress the differences between the versions of the same semantic image. Another state-of-the-art SSL branches are mask-based approaches that remove part of the input image and reconstruct them or a transformed version of them, either in the original image space [4, 23], or in the feature space [2]. Contrastive learning has been combined with the masked approach, but only pixel-accurate translation has been applied as augmentation [25]. As these methods do not, apart from masking or cropping, rely on other transformation, they are by construction more open for equivariance. Our approach is closely related to SIE [18], a method that combines the matching approach with an explicit model of transformations applied in the input space. Our approach can be seen as an extension which does not require knowledge about the transformation parameters, *i.e.* it can also be applied with respect to any transformations without the need to know them explicitly as long as one can apply them to the image. In contrast to SIE, our approach reaches state-of-the-art results.

2.3. Equivariance vs. invariance

A function, in our context represented by the deep learning model, between two spaces, the input image space in the context of computer vision tasks and the space of feature

presentations, is denoted as equivariant with respect to a transformation in the input space and a corresponding transformation in the output space, if the function commutes with the transformations, i.e. it does not matter if one first applies the transformation in the input space and then the function or first the mapping to the output space and then applies the corresponding transformation there. The definition includes the identity transformation in the output space such that invariance is always equivariance. However, in the computer vision literature *e.g.* [11, 14, 17, 20, 34, 37, 39], as we do in this paper, invariance is often opposed to equivariance to stress that all information about the transformation in the input space is still retrievable from the output space. The term equivariance is usually considered for a set of transformations, *i.e.* the function is said to be equivariant with respect to this set of transformations. Moreover, the set of transformations is considered a group transformation or, even stronger, a group representation of the transformation, *i.e.* a linear map, in the input and output space. However, not all transformations applied in computer vision can be modelled by group transformations like elastic distortions, crop-resize operations, or non-affine perspective transformations. In addition, transformations that can theoretically be formulated as group transformations might lose the corresponding group properties in practice, *e.g.*, an image rotated around a general angle cannot be rotated back as parts of the image get lost during the forward transformation. In this paper, we do not restrict the model to be equivariant with transformations that belong to a certain further structure but argue that equivariance is no value in itself but should serve as a property to help to learn a feature representation that contains all the information necessary for all kinds of downstream tasks. We do not restrict the transformation to form a group or require them to be linear in the feature space. Instead we motivate the model to maintain the information that is necessary to maintain input output relation such that transformed images in the input space can be retrieved by the representation irrespective if the transformation forms a linear transformation, a general group transformation, or even if the definition of equivariance is only approximately fulfilled in the feature representation. We denote this as equivariant-coherence.

3. Method

For augmentation-based SSL methods, joint embedding feature matching between two augmented images is commonly used to learn image features from unlabeled data. While these methods effectively capture invariant features, they require auxiliary tasks to learn equivariant features. Our approach draws inspiration from SIE [18], which splits features into invariant and equivariant components, using the equivariant part for auxiliary tasks to learn equivariant-coherent features. A detailed comparison between our

method and SIE is presented in Section 3.1.

In our proposed framework, depicted in Figure 1, we introduce transformation g as an additional augmentation applied exclusively to the second view $v_2 \in \mathbb{R}^{B \times 3 \times 224 \times 224}$, where B denotes the batch size. Both augmented views are processed by the encoder f , which shares weights during pretraining. The resulting feature representations $z \in \mathbb{R}^{B \times N \times d_{\text{patch_embed}}}$ are then divided into two distinct sets along patch embeddings, that is, the total patch embeddings $d_{\text{patch_embed}} = d_{\text{inv}} + d_{\text{equiv}}$, where N is the number of patches and $d_{\text{patch_embed}}$ is the dimension of patch embedding:

- **Invariant features** $z_{\text{inv}}^i \in \mathbb{R}^{B \times N \times d_{\text{inv}}}$: These features compute the self-supervised learning (SSL) loss based on the chosen method (*e.g.*, iBOT loss).
- **Equivariant features** $z_{\text{equiv}}^i \in \mathbb{R}^{B \times N \times d_{\text{equiv}}}$: These features are concatenated to reconstruct intermediate transformed images.

We employ two independent decoders, d_1 and d_2 , operating on the concatenated equivariant features to reconstruct intermediate transformed images, thereby computing the reconstruction loss L_{recon} .

It is combined with the SSL loss L_{SSL} using a weighting hyperparameter λ :

$$L_{\text{total}} = L_{\text{SSL}} + \lambda L_{\text{recon}} \quad (1)$$

Notably, the feature split ratio $|z_{\text{equiv}}|/|z_{\text{inv}}|$ between invariant and equivariant features is not necessarily one. We conduct sensitivity analyses to investigate how different splitting strategies affect equivariant feature learning.

3.1. Our Method vs. SIE [18]

In SIE, the exact transformation parameters between views are required for training and modeled as a linear mapping, which is then learned to align equivariant features across views. A key challenge in SIE is obtaining prior knowledge of these transformations, which is often impractical for natural images. To address this, we artificially introduce transformations such as rotation, color jittering, Gaussian blur, and translation, ensuring that the transformation parameters are known and allowing SIE to be applied to natural images.

In contrast, our method does not require knowledge of transformation parameters to train a model with equivariant features. Instead, we learn the natural variations between two augmented views. Incorporating spatial augmentations into the standard self-supervised learning augmentation pipeline with our approach effectively facilitates the learning of equivariant features, as demonstrated in Table 2.

3.2. Transformations

We introduce group transformations, approximate group transformation and non-group transformations in the reconstruction process to learn equivariant features. These group

Transformations g	Parameters	Mag. range
Rotation	angle θ	$[-45, 45]$
Color jittering	brightness B , contrast C , saturation S , hue H	$[-0.4, 0.4]$ $[-0.1, 0.1]$
Gaussian blur	radius σ	$[0.1, 2]$
Translation	displacement t_x, t_y	$[-10, 10]$
SE(2)	angle θ displacement t_x, t_y	$[-45, 45]$ $[-10, 10]$

Table 1. Considered transformations.

transformations include geometric transformations such as rotation, translation, and special Euclidean group transformations SE(2).

SE(2) defines the isometries in \mathbb{R}^2 that preserve the orientation, i.e. it combines 2d rotation and translation.

Additionally, we incorporate non-geometric transformations, including color jittering and Gaussian blur. The parameter magnitude ranges for these transformations are shown in Table 1.

We designed the decoder to be as simple as possible, compare yellow box in Figure 1. Specifically, we used a single linear layer to match the input dimensions of the subsequent four convolutional layers. Our goal is not to reconstruct perfect intermediate transformed images but to develop an encoder f that produces better equivariant representations. Therefore, the decoder d should not interfere with the learning of equivariance-coherent features during pretraining. We implemented two independent decoders for learning the intermediate reconstruction, with the number of decoders determined by the number of intermediate images. In the sensitivity analysis, we determine the optimal number of intermediate images, finding that 2 is optimal.

4. Experimental results

As our method builds on SIE [18], SIE is our first natural baseline with synthetic evaluation tasks designed to benefit from equivariant features. To evaluate the generalization of our method against state-of-the-art approaches, we go beyond using the invariant loss function L_{SSL} as in SIE and explore integrating other methods. Specifically, we incorporate co-learning with iBOT [45] and DINOv2 [33], both of which are augmentation-based techniques. They are also tested on the synthetic benchmark. Finally, we evaluate on a rich set of more realistic downstream tasks. We aim to enhance the baselines’ performance on equivariance-related tasks while preserving strong results on invariance-related benchmarks, e.g. ImageNet linear probing.

4.1. Implementation Details

Architecture. We use Vision Transformers (ViTs) [15] with different configurations, specifically ViT-S/16 and ViT-L/16, as our backbone architectures for experiments.

As the different baseline methods we compare to use different representation dimensions, i.e. 8192 for iBOT, 512 for SIE, and 2048 for DINOv2, we incorporate a linear head on top of the backbone to accommodate.

Afterwards, a portion z_{equi} of these features z is allocated for reconstruction; we do not introduce more features than the baseline methods.

Pretraining setup. Our approach uses a baseline SSL loss L_{SSL} in addition to our new component L_{recon} . Each of the three baseline methods come with distinct training setups. The common training configuration includes ImageNet-1K as the dataset, AdamW [31] as the optimizer, and a cosine-scheduled learning rate. For the SIE-based method, where we apply only their invariant loss as L_{SSL} , we pretrain ViT-S/16 for 800 epochs with a batch size of 2048. The base learning rate is set to $1e-4$ and is linearly scaled with the batch size: $lr = 1e-4 \times \frac{\text{batch_size}}{256}$. For the iBOT-based approach, we pretrain ViT-S/16 for 800 epochs and ViT-L/16 for 250 epochs, both with a batch size of 1024. The learning rate follows the same linear scaling strategy, with a base learning rate of $5e-4$. For the DINOv2-based training, we train ViT-L/16 with 100 epochs with batch size of 2048. The base learning rate is $4e-3$ with warmup 10 epochs.

4.2. Synthetic tasks

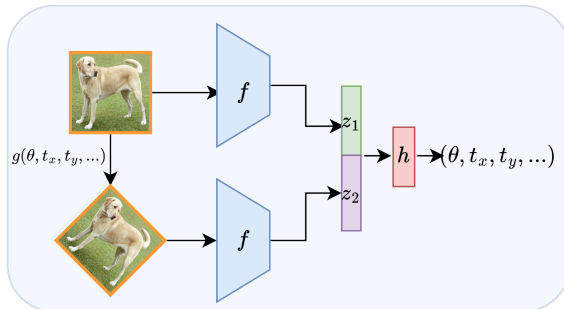


Figure 2. **Synthetic tasks for evaluating equivariant representations.** The transformation (g) is applied to the original image I , and both the transformed and original images are processed through a pretrained encoder f . A lightweight MLP h then predicts the parameters of the applied transformation.

Following [36], we design synthetic tasks to evaluate the equivariant representations learned during pretraining, see Figure 2. These regression-based tasks assess the transformation parameters between original and transformed views. Following the evaluation metrics used in SIE [18], we formulate transformation parameters prediction as a regression problem. To quantify alignment between predicted and true values, we use the coefficient of determination (R^2)

$$R^2 = 1 - \frac{RSS}{TSS} \quad (2)$$

where RSS is the sum of squared residuals, and TSS is

Configurations	R^2 (rot)	R^2 (color)	R^2 (blur)	R^2 (trans)	Mean(R^2)
SIE(rot)	<u>0.990</u>	0.867	0.042	0.540	0.610
SIE(color)	0.078	0.890	0.097	0.355	0.355
SIE(blur)	0.153	0.883	<u>0.941</u>	0.189	0.542
SIE(trans)	0.213	0.885	0.023	<u>0.978</u>	0.525
SIE(all)	0.331 ± 0.007	0.899 ± 0.003	0.211 ± 0.005	0.925 ± 0.002	0.592
Cross atten recon [36]	0.893 ± 0.004	<u>0.921</u> ± 0.006	0.823 ± 0.030	0.875 ± 0.005	0.878
Ours(SIE, rot, rot)	0.9975 ± 0.0005	0.9073 ± 0.0021	0.9310 ± 0.0020	0.9810 ± 0.0010	0.954
Ours(SIE, all, rot)	0.9983 ± 0.0005	0.9231 ± 0.0005	0.9689 ± 0.0099	0.9801 ± 0.0004	0.968
Ours(SIE, all, color)	0.9891 ± 0.0019	0.9373 ± 0.0013	0.9700 ± 0.0067	0.9699 ± 0.0022	0.967
Ours(SIE, all, blur)	0.9981 ± 0.0001	0.9154 ± 0.0006	0.9392 ± 0.0106	0.9774 ± 0.0007	0.958
Ours(SIE, all, trans)	0.9975 ± 0.0005	0.9288 ± 0.0012	0.9747 ± 0.0017	0.9830 ± 0.0004	0.971
Ours(SIE, all, se(2))	0.9980 ± 0.0001	0.9158 ± 0.0005	0.9520 ± 0.0050	0.9740 ± 0.0001	0.960

Table 2. **Comparison of R^2 values across different configurations for synthetic tasks.** Text in brackets in the configuration names indicate (1) for SIE the training transformation (cmp. Table 1) and (2) for Ours the first entry indicates the invariant loss, the second the augmentation applied to the input image, the third the transformation of the reconstruction asked for in L_{recon} . We apply either rotation as the sole augmentation or a combination of all augmentations (rot or all) and infer intermediate transformations such as angle, color, blur, and translation. Bold values indicate the best overall, while underlined values represent the best among baseline methods.

the total sum of squares. A higher R^2 value indicates more accurate transformation predictions.

4.2.1. Comparison with other SIE-based methods

For this experiment, we use ViT-S/16 for all methods. Our method (Ours) uses the SIE-configuration and the SIE invariant loss for L_{SSL} . We compare with SIE [18] and a closely related cross-attention-based reconstruction method [36], see Table 2. For SIE, the performance with single augmentations and prior knowledge is the best among the baseline methods, but for color jitter estimation, where all variants perform well. However, it generalizes poorly to other transformation evaluations (best mean 0.610). While cross-attention reconstruction [36] leads to much more balanced results (mean 0.878), its performance does not surpass SIE with single augmentations, but for color. For our method, we tested different combinations of augmentation and intermediate transformation. All of them show a strong average performance increase (mean from 0.954 to 0.971 compared to 0.878 for the cross attention method [36]). The best ones, i.e. Ours(SIE, all, rot) and Ours(SIE, all, trans), even outperform all competitors on all tasks individually.

4.2.2. Enhancing the transformation prediction of SOTA augmentation-based SSL methods

We test pretrained state-of-the-art ViT-L/16 models on the same rotation and color jitter prediction task (as outlined in 4.2), see Table 3. The baseline iBOT [45] pretrained model is taken from the official repository. For fair comparison, numbers shown for the DINOv2 baseline model are for a model we pretrained from scratch, as it performed better than with the weights from the official repository. For color prediction, iBOT and DINOv2 perform on par with the smaller ViT-S/16 models from Table 2; we repeated the entries for SIE(rot), SIE(all), and Ours(SIE, all, rot), for

convenience. However, DINOv2 and iBOT perform significantly worse on the rotation estimation task. Training them from scratch using our approach improves their performance to best-in-class for color prediction (Ours(iBOT, all, se(2))). For rotation prediction, improvements for iBOT are remarkably high from 0.238 to 0.937. DINOv2 performance is also improved, but much less and to a lower performance (0.84). Notably, using se(2) as intermediate transform for iBOT and DINOv2 works slightly better than rotation, in contrast to SIE, see Table 2.

Configuration or Method	Rotation	Color
SIE(rot)	0.990	0.867
SIE(all)	0.331	0.899
iBOT	0.238	0.913
DINOv2	0.774	0.910
Ours(SIE, all, rot)	0.997 (↑0.007)	0.923 (↑0.056)
Ours(iBOT, all, rot)	0.925 (↑0.687)	0.934 (↑0.021)
Ours(iBOT, all, se(2))	0.937 (↑0.699)	0.943 (↑0.030)
Ours(DINOv2, all, rot)	0.812 (↑0.038)	0.920 (↑0.010)
Ours(DINOv2, all, se(2))	0.840 (↑0.066)	0.933 (↑0.023)

Table 3. Performance comparison on rotation and color prediction tasks with improvements of our methods (absolute values). See Table 2 for description of configuration names. Rows with the same color represent the baseline results used for comparison with our methods.

4.3. Performance on natural images tasks

Our method demonstrates strong performance on the synthetic tasks discussed above, motivating us to explore its impact on real-world imaging tasks commonly studied in self-supervised learning (SSL). We aim to achieve results on par with state-of-the-art approaches, when downstream tasks are not to be expected to benefit from equivariance,

like classification tasks. We strive to identify tasks where equivariant features are particularly beneficial.

Unless said differently, we use our method with iBOT and DINOv2 configurations performing best on the synthetic tasks from Table 3, i.e. Ours(iBOT, all, se(2)) and Ours(DINOv2, all, se(2)). Below, we call them Ours(iBOT) and Ours(DINOv2), respectively.

4.3.1. Linear probing on Classification tasks

In this study, we follow the standard self-supervised learning evaluation pipeline, where the pretrained network is frozen, and only the linear head is fine-tuned on downstream tasks. The results, as shown in Table 4 and visualized in Figures 3 and 4, are based on models pretrained on ImageNet1k. While we expected our results to be comparable to the baseline for all invariant tasks, we were pleasantly surprised to find that our method improved performance compared to the baselines on average and across most datasets and tasks. Specifically, Ours(DINOv2) consistently achieved superior performance, with notable improvements in CIFAR10 (98.91% vs. 98.47%), CIFAR100 (90.37% vs. 89.28%), and Aircraft (71.64% vs. 70.89%), surpassing DINOv2 and other baselines. In contrast, only on the Food dataset our method fell slightly behind Ours(iBOT) (88.66% vs. 87.80%), which still represented a competitive result. Furthermore, SIE methods, which focus on equivariant features, did not perform well on natural image classification tasks. As a result, we focused on iBOT and DINOv2-related methods in later experiments.

4.3.2. Transfer learning tasks

We investigate multiple downstream tasks that leverage equivariant features, including semantic segmentation, object detection, keypoint detection, and homography estimation. For semantic segmentation, we fine-tune our pretrained model using UPerNet [38]. For instance segmentation and object detection, we employ Mask R-CNN [21] with our pretrained model. Finally, for homography estimation, we design a 3-layer convolutional head to output the displacement map.

Based on the results presented in Tables 5, visualized in Figures 3 and 4, our method demonstrates strong performance across a variety of dense prediction tasks, including semantic segmentation (ADE20k [44]), object detection (CoCo det [30]), instance segmentation (CoCo ins [30]), keypoint detection (CoCo key [30], MPii key [1]), and homography estimation (S-CoCo [13]). Specifically, in Table 5, our approach (Ours(DINOv2)) outperforms the baseline methods, iBOT and DINOv2, in several cases, with a notable improvement in ADE20k (0.5412 vs. 0.5349, mIOU). Additionally, our method (Ours(DINOv2)) achieves the best performance in the S-CoCo-finetune task with a Mean Corner Error (MCE) of 1.42, outperforming both iBOT (1.76) and DINOv2 (1.68). These results demonstrate the

effectiveness of equivariant features in enhancing the performance of practical computer vision applications, confirming that our method provides positive improvements over existing SOTA self-supervised learning techniques.

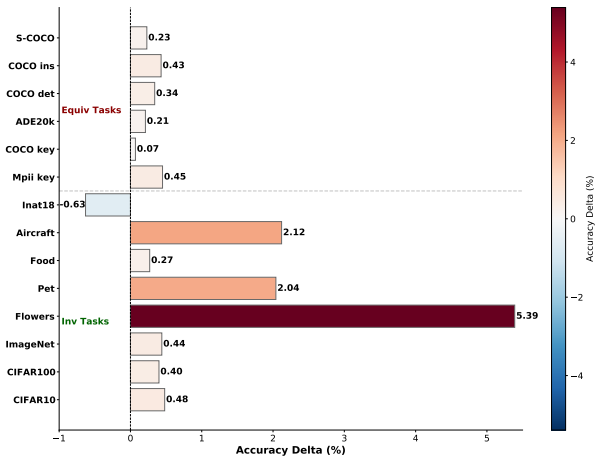


Figure 3. Absolute accuracy difference compared to iBOT among downstream tasks. Pretrained with SE(2) reconstruction.

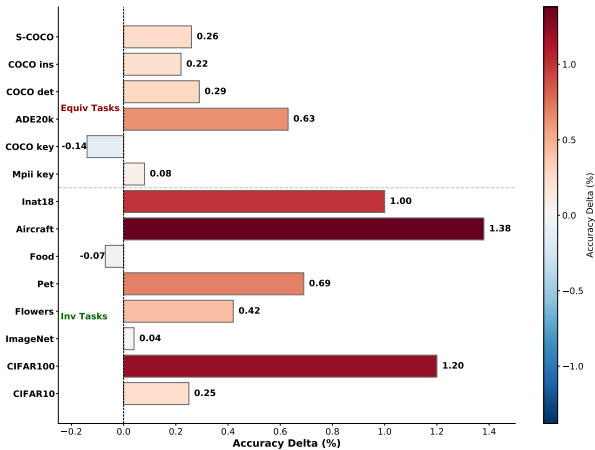


Figure 4. Absolute accuracy difference compared to DINOv2 among downstream tasks. Pretrained with SE(2) reconstruction.

4.4. Comparison with augmentation-free methods

We compare our approach with reconstruction-based self-supervised learning (SSL) methods that require minimal augmentations, such as MAE [24], and those that require no augmentations, such as I-JEPA [2]. From Figure 5, we observe that all augmentation-based feature-matching methods (DINO [6], DINOv2 [33], MoCo [9]) perform poorly on rotation prediction tasks, yielding worse results compared to reconstruction-based methods (MAE, I-JEPA). However, our approach enhances the performance of augmentation-based invariance matching methods on both tasks.

Configuration or Method	CIFAR10	CIFAR100	Aircraft	Pet	Food	Flowers	INat18	ImageNet
IBOT	97.60%	86.96%	55.43%	92.30%	88.39%	90.64%	57.30%	81.00%
DINOv2	98.47%	89.28%	70.89%	94.82%	87.92%	96.39%	69.42%	82.60%
Ours(IBOT, all, se(2))	98.08%	87.36%	57.55%	94.34%	88.66%	96.03%	57.99%	81.44%
Ours(DINOv2, all, se(2))	98.91%	90.37%	71.64%	95.42%	87.80%	96.81%	70.41%	82.73%

Table 4. Performance comparison on classification datasets. Please see Table 2 for the naming convention.

Method	ADE20k	CoCo det	CoCo ins
	mIoU	AP ^b	AP ^m
IBOT	0.5217	0.5158	0.4448
DINOv2	0.5349	0.5303	0.4574
Ours (IBOT)	0.5238	0.5192	0.4478
Ours (DINOv2)	0.5412	0.5332	0.4596

Method	CoCo key	MPii key	S-CoCo _↓
	mAP	PCKh	MCE
IBOT	0.7364	0.8697	1.76
DINOv2	0.7512	0.8728	1.68
Ours (IBOT)	0.7371	0.8742	1.53
Ours (DINOv2)	0.7498	0.8736	1.42

Table 5. Performance comparison on dense prediction datasets. The symbol \downarrow denotes that lower values are considered better.

We see that the reconstruction-based methods in Figure 5 (MAE, I-JEPA) perform well on transformation prediction tasks. However, they are based on larger models such as ViT-H and ViT-G and/or pretraining on large-scale datasets like ImageNet-22K. In contrast, our approach uses ViT-S and still achieves results comparable to these larger models.

One limitation of reconstruction-based methods is their weaker performance on invariance-related tasks, as shown in Table 6. When evaluated with linear probing, MAE and I-JEPA perform worse than or at best on par with augmentation-based methods iBOT and DINOv2, even though MAE and I-JEPA models are much larger. Our method improves slightly but consistently on the iBOT and DINOv2 baselines with the same model and training data.

We conclude that our results demonstrate that by incorporating transformation reconstruction, our method preserves equivariant representations like reconstruction approaches—and even slightly outperforms augmentation-based methods on invariant tasks.

4.5. Sensitivity analysis

Our method involves several hyperparameters: the split dimension d of z_{equi} for transformation reconstruction, the weight λ in (1) for the equivariant loss L_{recon} , the number of intermediate images for reconstruction, and the transformations required for the reconstructions. We use iBOT and the small ViT-s/16 for this sensitivity analysis to minimize computational load. Specifically, for the split dimension d and the loss weight λ , we performed pretraining for 100

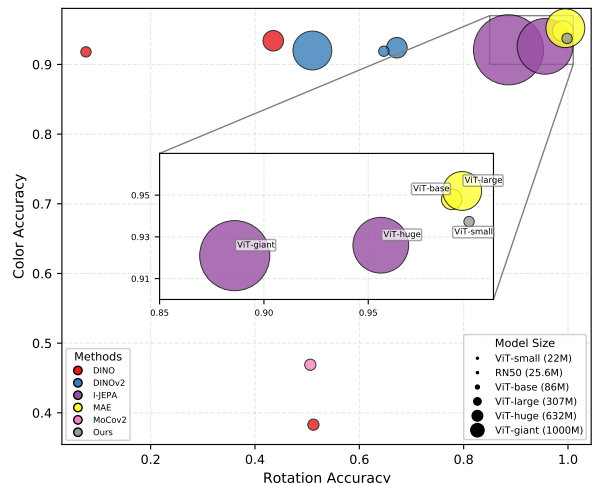


Figure 5. Synthetic tasks results among SSL methods

Method	Pretrain	Arch.	CIFAR100	iNat18	ImageNet
MAE[24]	IN1k	ViT-H/14	77.3	32.9	77.2
I-JEPA[2]	IN1k	ViT-H/14	87.5	47.6	77.5
I-JEPA[2]	IN22k	ViT-H/14	89.5	50.5	79.3
I-JEPA[2]	IN22k	ViT-G/16	89.5	55.3	-
iBOT	IN1k	ViT-L/16	87.0	57.3	81.0
DINOv2	IN1k	ViT-L/16	89.3	69.4	82.6
DINOv2[33]	LVD-142M	ViT-g/14	94.0	81.6	87.1
Ours(iBOT)	IN1k	ViT-L/16	87.8	58.0	81.6
Ours(DINOv2)	IN1k	ViT-L/16	90.4	70.4	82.7

Table 6. Invariant tasks comparison to models that require no augmentations.

epochs. For transformation analysis, we extended the pre-training to 800 epochs. We use SE(2) transformation if not said differently.

4.5.1. Split dimension d and loss weight λ

We selected all combinations from $\lambda \in \{0.1, 1.0, 5.0\}$ and $d \in \{256, 512, 1024, 2048, 4096, 5120\}$ pretrained on ImageNet-1k as described above. We also tested $\lambda > 5.0$, and observed the training process to become unstable. We tested all models on all datasets and tasks from Tables 5 and 4. We report means and variances over classification tasks in Figure 6b and from equivariance-related tasks in Figure 6a. From Figure 6a, we can conclude that the mean performance of the equivariance-related tasks improves with increasing λ . Dimension d has a notable effect only for $\lambda = 1.0$, where $d = 4096$ performs best, i.e. using half

of the features. For invariant tasks, Figure 6b, only models with $\lambda \leq 1.0$ yield mainly the same performance as the baseline iBOT. We observe improved performance only for $d = 2048$ and $\lambda = 0.1$. Notably, for $\lambda = 5.0$ invariance-related tasks’ performance remains undisturbed, while equivariance-related tasks well improve.

We conclude that, as expected, equivariance-related tasks benefit from higher λ and higher d , while invariance-related tasks remain unharmed with lower λ and lower d . Sweet spots are small λ and $d = 2048$ and at large λ and small $d = 256$. We selected $\lambda = 1$ and $d = 2048$ for our experiments.

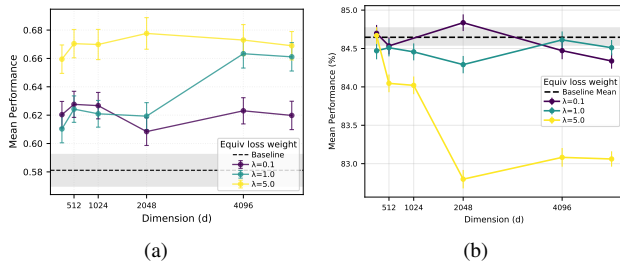


Figure 6. Mean performance of (a) equivariance-related tasks and (b) invariance-related tasks.

4.5.2. Transformations analysis

For in-between inference, we implement three types of geometric transformations: rotation only, translation only, and SE(2), i.e. the combination of rotation and translation. Results for these transformations are presented in Figure 7. Our findings indicate that rotation yields the best performance among the three for invariant tasks. Notably, for INat18, only the rotation transformation surpasses the baseline. In contrast, for equivariant tasks, SE(2) consistently achieves the best performance across all tasks. While the intermediate reconstruction using rotation does not perform as well as the other two transformations, it still outperforms the baseline. Furthermore, the performance improvement margin for equivariant-related works is not as large as for invariant tasks. This is because we apply linear probing to invariant tasks, whereas we use fine-tuning for equivariant tasks. The lower improvement margin for fine-tuning compared to linear probing can be attributed to the difference in flexibility and capacity for adaptation. In linear probing, only a small classifier head is trained on top of frozen pre-trained features, meaning the model relies entirely on the quality of the learned representations. If the in-between inference transformation enhances these representations, the improvement can be significant because the classifier has limited capacity to compensate for suboptimal features.

In contrast, fine-tuning updates the entire model, allowing it to adjust its representations to the specific task. As a result, the benefits of in-between inference transformations

are less pronounced since the model can already learn to adapt through parameter updates. This leads to a smaller performance gap than the baseline, as the model’s capacity to optimise itself reduces its reliance on improved intermediate representations.

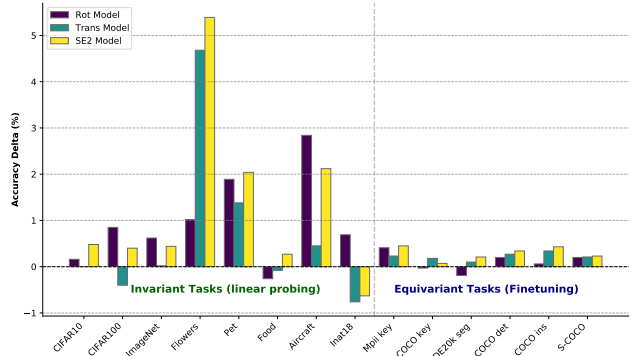


Figure 7. Downstream tasks evaluation for different inference strategies.

4.5.3. Number of inbetween images

We investigate the effects of the number of in-between images, with the results presented in Table 7. We observe that with only one in-between image, the performance is suboptimal. However, as the number of intermediate images increases to two, the performance on synthetic tasks improves significantly. Notably, adding more than two in-between images or incorporating the augmented view v_2 for reconstruction does not lead to further improvements. Considering both performance gains and GPU memory constraints, we select two in-between images for our experiments.

# of Images	R^2 (rot)	R^2 (color)	R^2 (blur)	R^2 (trans)
1	0.2915	0.4708	0.8725	0.4230
2	0.9983	0.9373	0.9689	0.9801
3	0.9981	0.9215	0.9506	0.9795
2+final	0.9981	0.9311	0.9562	0.9771

Table 7. Number of Inbetween images investigation. The model is Ours(SIE, all, rot), cmp. Table 2.

5. Summary and Conclusions

We propose a novel approach for augmentation-based SSL methods that enhances the learning of equivariant-coherent features by reconstructing intermediate representations of transformed images. Our method significantly boosts performance on equivariance-focused synthetic tasks and surpasses competitors like SIE. Moreover, we achieve comparable or superior results on real-world imaging tasks using iBOT and DINOv2 as base methods. This approach provides a promising direction for improving the generaliza-

tion of SSL methods and can be easily adapted to other SSL frameworks.

6. Acknowledgements

The authors gratefully acknowledge the Gauss Centre for Supercomputing e.V. (www.gauss-centre.eu) for funding this project by providing computing time through the John von Neumann Institute for Computing (NIC) on the GCS Supercomputer JUWELS [27] at Jülich Supercomputing Centre (JSC).

References

- [1] Mykhaylo Andriluka, Leonid Pishchulin, Peter Gehler, and Bernt Schiele. 2d human pose estimation: New benchmark and state of the art analysis. In *2014 IEEE Conference on Computer Vision and Pattern Recognition*, pages 3686–3693, 2014. 6
- [2] Mahmoud Assran, Quentin Duval, Ishan Misra, Piotr Bojanowski, Pascal Vincent, Michael G. Rabbat, Yann LeCun, and Nicolas Ballas. Self-supervised learning from images with a joint-embedding predictive architecture. *2023 IEEE/CVF Conference on Computer Vision and Pattern Recognition (CVPR)*, pages 15619–15629, 2023. 1, 2, 6, 7
- [3] Randall Balestriero, Mark Ibrahim, Vlad Sobal, Ari Morcos, Shashank Shekhar, Tom Goldstein, Florian Bordes, Adrien Bardes, Gregoire Mialon, Yuandong Tian, Avi Schwarzschild, Andrew Gordon Wilson, Jonas Geiping, Quentin Garrido, Pierre Fernandez, Amir Bar, Hamed Pirsiavash, Yann LeCun, and Micah Goldblum. A cookbook of self-supervised learning, 2023. 2
- [4] W. G. C. Bandara, Naman Patel, Ali Gholami, Mehdi Nikkiah, Motilal Agrawal, and Vishal M. Patel. Adamae: Adaptive masking for efficient spatiotemporal learning with masked autoencoders. *2023 IEEE/CVF Conference on Computer Vision and Pattern Recognition (CVPR)*, pages 14507–14517, 2022. 2
- [5] Adrien Bardes, Jean Ponce, and Yann LeCun. Vircreg: Variance-invariance-covariance regularization for self-supervised learning, 2022. 2
- [6] Mathilde Caron, Hugo Touvron, Ishan Misra, Hervé Jegou, Julien Mairal, Piotr Bojanowski, and Armand Joulin. Emerging properties in self-supervised vision transformers. In *2021 IEEE/CVF International Conference on Computer Vision (ICCV)*, pages 9630–9640, 2021. 6
- [7] Mathilde Caron, Hugo Touvron, Ishan Misra, Hervé Jégou, Julien Mairal, Piotr Bojanowski, and Armand Joulin. Emerging properties in self-supervised vision transformers, 2021. 2
- [8] Ting Chen, Simon Kornblith, Mohammad Norouzi, and Geoffrey Hinton. A simple framework for contrastive learning of visual representations, 2020. 1
- [9] Xinlei Chen, Haoqi Fan, Ross Girshick, and Kaiming He. Improved baselines with momentum contrastive learning. *arXiv preprint arXiv:2003.04297*, 2020. 1, 2, 6
- [10] Taco S. Cohen and Max Welling. Steerable CNNs, 2016. 2
- [11] Rumen Dangovski, Li Jing, Charlotte Loh, Seung-Jun Han, Akash Srivastava, Brian Cheung, Pulkit Agrawal, and βMarin Soljačić. Equivariant contrastive learning. *ArXiv*, abs/2111.00899, 2021. 2, 3
- [12] Jia Deng, Wei Dong, Richard Socher, Li-Jia Li, Kai Li, and Li Fei-Fei. Imagenet: A large-scale hierarchical image database. In *2009 IEEE Conference on Computer Vision and Pattern Recognition*, pages 248–255, 2009. 1
- [13] Daniel DeTone, Tomasz Malisiewicz, and Andrew Rabynovich. Deep image homography estimation. *ArXiv*, abs/1606.03798, 2016. 6
- [14] Alexandre Devillers and Mathieu Lefort. Equimod: An equivariance module to improve visual instance discrimination. In *International Conference on Learning Representations*, 2022. 3
- [15] Alexey Dosovitskiy, Lucas Beyer, Alexander Kolesnikov, Dirk Weissenborn, Xiaohua Zhai, Thomas Unterthiner, Mostafa Dehghani, Matthias Minderer, Georg Heigold, Sylvain Gelly, Jakob Uszkoreit, and Neil Houlsby. An image is worth 16x16 words: Transformers for image recognition at scale. *ArXiv*, abs/2010.11929, 2020. 4
- [16] Kuniyuki Fukushima. Neocognitron: A self-organizing neural network model for a mechanism of pattern recognition unaffected by shift in position. *Biological Cybernetics*, 36: 193–202, 1980. 2
- [17] Quentin Garrido, Laurent Najman, and Yann LeCun. Self-supervised learning of split invariant equivariant representations. *ArXiv*, abs/2302.10283, 2023. 3
- [18] Quentin Garrido, Laurent Najman, and Yann LeCun. Self-supervised learning of split invariant equivariant representations. In *Proceedings of the 40th International Conference on Machine Learning (ICML)*, 2023. 2, 3, 4, 5
- [19] Spyros Gidaris, Praveer Singh, and Nikos Komodakis. Unsupervised representation learning by predicting image rotations. *ArXiv*, abs/1803.07728, 2018. 2
- [20] Sharut Gupta, Joshua Robinson, Derek Lim, Soledad Villar, and Stefanie Jegelka. Structuring representation geometry with rotationally equivariant contrastive learning. *ArXiv*, abs/2306.13924, 2023. 3
- [21] Kaiming He, Georgia Gkioxari, Piotr Dollár, and Ross Girshick. Mask r-cnn. In *2017 IEEE International Conference on Computer Vision (ICCV)*, pages 2980–2988, 2017. 6
- [22] Kaiming He, Haoqi Fan, Yuxin Wu, Saining Xie, and Ross Girshick. Momentum contrast for unsupervised visual representation learning, 2020. 1, 2
- [23] Kaiming He, Xinlei Chen, Saining Xie, Yanghao Li, Piotr Dollár, and Ross Girshick. Masked autoencoders are scalable vision learners. In *Proceedings - 2022 IEEE/CVF Conference on Computer Vision and Pattern Recognition, CVPR 2022*, pages 15979–15988. IEEE Computer Society, 2022. Publisher Copyright: © 2022 IEEE.; 2022 IEEE/CVF Conference on Computer Vision and Pattern Recognition, CVPR 2022 ; Conference date: 19-06-2022 Through 24-06-2022. 2
- [24] Kaiming He, Xinlei Chen, Saining Xie, Yanghao Li, Piotr Dollár, and Ross Girshick. Masked autoencoders are scalable vision learners. In *Proceedings of the IEEE Conference on Computer Vision and Pattern Recognition (CVPR)*, pages 15979–15988, 2022. 1, 6, 7
- [25] Zhicheng Huang, Xiaojie Jin, Cheng Lu, Qibin Hou, Mingming Cheng, Dongmei Fu, Xiaohui Shen, and Jiashi Feng.

- Contrastive masked autoencoders are stronger vision learners. *IEEE Transactions on Pattern Analysis and Machine Intelligence*, 46:2506–2517, 2022. 2
- [26] Erik Jenner and Maurice Weiler. Steerable partial differential operators for equivariant neural networks. In *International Conference on Learning Representations*, 2022. 2
- [27] Jülich Supercomputing Centre. JUWELS Cluster and Booster: Exascale Pathfinder with Modular Supercomputing Architecture at Juelich Supercomputing Centre. *Journal of large-scale research facilities*, 7(A138), 2021. 9
- [28] Diederik P. Kingma and Jimmy Ba. Adam: A method for stochastic optimization. *CoRR*, abs/1412.6980, 2014. 11
- [29] Johannes Lehner, Benedikt Alkin, Andreas Fürst, Elisabeth Rumetshofer, Lukas Miklautz, and Sepp Hochreiter. Contrastive tuning: A little help to make masked autoencoders forget, 2023. 2
- [30] Tsung-Yi Lin, Michael Maire, Serge Belongie, Lubomir Bourdev, Ross Girshick, James Hays, Pietro Perona, Deva Ramanan, C. Lawrence Zitnick, and Piotr Dollár. Microsoft coco: Common objects in context, 2015. 6, 11
- [31] Ilya Loshchilov and Frank Hutter. Decoupled weight decay regularization. In *International Conference on Learning Representations*, 2017. 4, 11
- [32] Mehdi Noroozi and Paolo Favaro. Unsupervised learning of visual representations by solving jigsaw puzzles. *ArXiv*, abs/1603.09246, 2016. 2
- [33] Maxime Oquab, Timothée Darcet, Théo Moutakanni, Huy Q. Vo, Marc Szafraniec, Vasil Khalidov, Pierre Fernandez, Daniel Haziza, Francisco Massa, Alaaeldin El-Nouby, Mahmoud Assran, Nicolas Ballas, Wojciech Galuba, Russ Howes, Po-Yao (Bernie) Huang, Shang-Wen Li, Ishan Misra, Michael G. Rabbat, Vasu Sharma, Gabriel Synnaeve, Huijiao Xu, Hervé Jégou, Julien Mairal, Patrick Labatut, Armand Joulin, and Piotr Bojanowski. DINOv2: Learning robust visual features without supervision. *ArXiv*, abs/2304.07193, 2023. 1, 2, 4, 6, 7
- [34] Jung Yeon Park, Ondrej Biza, Linfeng Zhao, Jan-Willem van de Meent, and Robin Walters. Learning symmetric embeddings for equivariant world models. In *International Conference on Machine Learning*, 2022. 3
- [35] Juergen Schmidhuber. Deep learning in neural networks: An overview. *Neural Networks*, 61, 2014. 1
- [36] Qin Wang, Kai Krajssek, and Hanno Schar. Equivariant representation learning for augmentation-based self-supervised learning via image reconstruction, 2024. 1, 4, 5
- [37] Yifei Wang, Kaiwen Hu, Sharut Gupta, Ziyu Ye, Yisen Wang, and Stefanie Jegelka. Understanding the role of equivariance in self-supervised learning. *ArXiv*, abs/2411.06508, 2024. 2, 3
- [38] Tete Xiao, Yingcheng Liu, Bolei Zhou, Yuning Jiang, and Jian Sun. Unified perceptual parsing for scene understanding. In *Computer Vision – ECCV 2018: 15th European Conference, Munich, Germany, September 8–14, 2018, Proceedings, Part V*, page 432–448, Berlin, Heidelberg, 2018. Springer-Verlag. 6, 11
- [39] Tete Xiao, Xiaolong Wang, Alexei A. Efros, and Trevor Darrell. What should not be contrastive in contrastive learning. *ArXiv*, abs/2008.05659, 2020. 2, 3
- [40] Johnathan Xie, Yoonho Lee, Annie S. Chen, and Chelsea Finn. Self-guided masked autoencoders for domain-agnostic self-supervised learning. *ArXiv*, abs/2402.14789, 2024. 2
- [41] Hengyuan Xu, Liyao Xiang, Hang Ye, Dixi Yao, Pengzhi Chu, and Baochun Li. Permutation equivariance of transformers and its applications. *2024 IEEE/CVF Conference on Computer Vision and Pattern Recognition (CVPR)*, pages 5987–5996, 2023. 2
- [42] Jure Zbontar, Li Jing, Ishan Misra, Yann LeCun, and Stéphane Deny. Barlow twins: Self-supervised learning via redundancy reduction, 2021. 2
- [43] Rui Zeng, Simon Denman, Sridha Sridharan, and Clinton Fookes. Rethinking planar homography estimation using perspective fields. In *Computer Vision - ACCV 2018: 14th Asian Conference on Computer Vision, Revised Selected Papers, Part VI (Lecture Notes in Computer Science, Volume 11366)*, pages 571–586. Springer, Switzerland, 2019. 11
- [44] Bolei Zhou, Hang Zhao, Xavier Puig, Sanja Fidler, Adela Barriuso, and Antonio Torralba. Scene parsing through ade20k dataset. In *2017 IEEE Conference on Computer Vision and Pattern Recognition (CVPR)*, pages 5122–5130, 2017. 6, 11
- [45] Jinghao Zhou, Chen Wei, Huiyu Wang, Wei Shen, Cihang Xie, Alan Yuille, and Tao Kong. iBOT: Image BERT pre-training with online tokenizer. *International Conference on Learning Representations (ICLR)*, 2022. 1, 2, 4, 5, 11

A. Appendix/supplemental material

A.1. Implementation details on downstream tasks

A.1.1. Linear probing.

For linear probing, the pretrained model remains frozen, and only the linear head is fine-tuned. We explore different configurations for the linear head:

1. Using only the [CLS] token.
2. Averaging patch embeddings.
3. Combining the average of patch embeddings with the [CLS] token.

Following iBOT [45], we use only [CLS] for ViT-S/16, whereas for larger models like ViT-L/16, we adopt strategy (3).

Besides, we use AdamW [31] as the optimizer, with a batch size of 1024 for all our downstream classification tasks. We all crop/scale the images into $3 \times 224 \times 224$ in the training process.

A.1.2. ADE20K [44] semantic segmentation

For all experiments involving ADE20K, we employed UPerNet [38] as the segmentation head. The output block indices for the encoder are [7, 11, 15, 23] for ViT-L/16 and [3, 5, 7, 11] for ViT-S/16. The input has a batch size of 8 and is cropped to $3 \times 224 \times 224$. For all backbones, we train the segmentor for 160k iterations using the AdamW optimizer. For ViT-S/16, the learning rate is set to $3e - 5$ with a layer decay rate of 0.9. For ViT-L/16, we use a learning rate of $2e - 5$ with a layer decay rate of 0.95.

The primary evaluation metric for ADE20K is mean Intersection over Union (mIoU), which measures the average overlap between predicted and ground truth segmentations across all classes.

A.1.3. COCO [30] detection and instance segmentation

We use the same output indices, optimizer, and layer decay as described in A.1.2. Given that the average aspect ratio of COCO is approximately 1.25, we adopt a larger crop size with the same ratio, setting it to (800×1008) . For ViT-L/16, we set the learning rate to $1e - 4$, while for ViT-S/16, we adjust the layer decay rate to 0.8. All experiments are conducted for 36 epochs.

For COCO instance segmentation and object detection, the standard evaluation metrics are based on mean Average Precision (mAP), as defined in the COCO evaluation protocol.

A.1.4. COCO and MPii Key point detection

We use a batch size of 512 for both datasets. All experiments are conducted using the Adam optimizer [28] with a learning rate of 0.0005. To evaluate model performance, we adopt pCKh (Percentage of Correct Keypoints with head-normalized tolerance), which measures the accuracy of predicted keypoints by determining whether they fall within a

specified threshold distance from the ground truth, normalized by head size.

A.1.5. Homography estimation, S-COCO [43]

We follow the same synthetic homography estimation task generation as [43]. The input images are converted to grayscale, and to match the required input dimensions, we replicate the single-channel input across three channels. We use the same crop size as the reference (112×112). The Adam optimizer is used for this task, with a batch size of 512.

The evaluation metric is Mean Corner Error (MCE), which measures the average euclidean distance between the predicted and ground truth corner points.

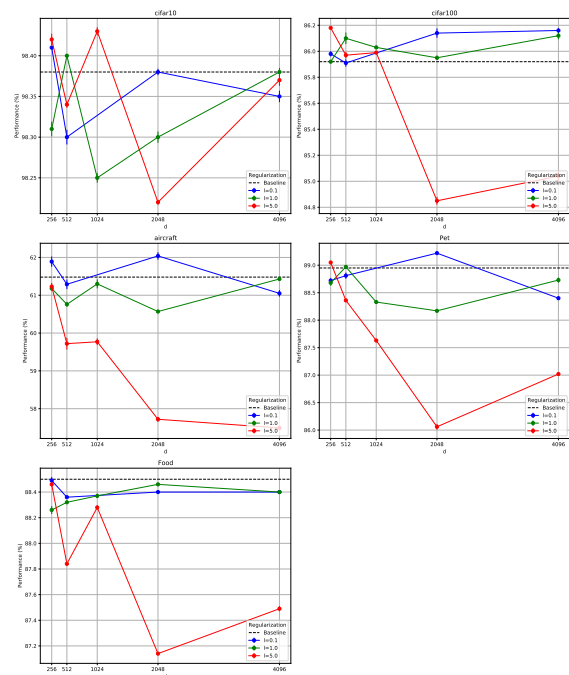


Figure 8. Equivariance loss weight and dimension hyperparameters for tasks related to the invariant representations

A.2. Sensitivity analysis on single dataset

Hyperparameter optimization for individual datasets is more complex. However, we can still conclude that for invariant tasks, as shown in Figure 8, careful selection of the weight scale is crucial. If the weight scale is too large, the network places greater emphasis on equivariant representations, leading to a drop in performance as the weight of the equivariance loss increases. Conversely, when using a smaller portion of equivariance learning, even with a larger weight, we still achieve strong results on invariant tasks.

For equivariant tasks, setting the weight to $l = 1l=1$ consistently yields strong performance across most datasets.

Notably, as the proportion of equivariant features increases, performance also scales accordingly.

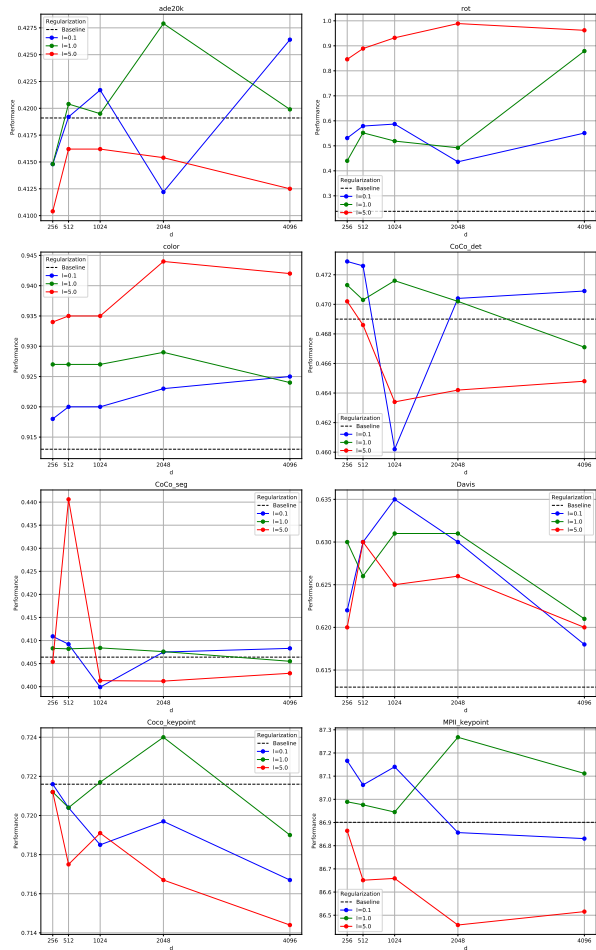


Figure 9. Equivariance loss weight and dimension hyperparameters for tasks related to the equivariant representations